NUSense: Shear Based Robust Optical Tactile Sensor

by

Madina Turmagambetova

Submitted to the Department of Robotics
in partial fulfillment of the requirements for the degree of

Master of Science in Robotics

at the

NAZARBAYEV UNIVERSITY

Apr 2025

Author .....
Department of Robotics
Apr 29, 2025

Certified by .....
Zhanat Kappassov
Associate Professor
Thesis Supervisor

Accepted by .....
Vassilios D. Tourassis
Dean, School of Engineering and Digital Sciences

NUSense: Shear Based Robust Optical Tactile Sensor

by

Madina Turmagambetova

Submitted to the Department of Robotics
on Apr 29, 2025, in partial fulfillment of the
requirements for the degree of
Master of Science in Robotics

Abstract

In this study, a new optical tactile sensing method that focuses on detecting shear strain rather than just pressure, which is traditionally used in most tactile sensors is presented. Drawing from principles in continuum mechanics, the importance of shear strain as a key parameter in tactile perception is highlighted. This work approach involves a layer of silicone rubber dyed with colored ink to visualize and measure the magnitude of shear deformation. To validate the concept, the NUSense optical tactile sensor was created, which integrates a wide-angle camera to observe the deformation of the soft layer when subjected to external forces. The deformation—mainly elongation due to the Poisson effect—is captured optically, offering insights into the shear behavior of the material. Since the accuracy of the sensor depends heavily on the long-term stability of the silicone's mechanical and optical properties, repeated loading tests using a robotic arm to evaluate durability and consistency were performed. How this sensing method could be applied to tasks such as force estimation and determining contact positions was explored, potentially expanding its use in robotic manipulation and soft interaction interfaces.

Thesis Supervisor: Zhanat Kappassov
Title: Associate Professor

Acknowledgments

The author acknowledges the enormous support of the thesis supervisor, Associate Professor Zhanat Kappassov.

The author extends heartfelt thanks to:

- Tleukhan Mussin
- Daryn Kenzhebek
- Saltanat Seitzhan
- Togzhan Syrymova

for their contribution to the development of NUSense.

The author would also like to express sincere gratitude to the following individuals and institutions:

Worldwide Researchers:

- Tasbolat Taunyazov, PhD., National Univ. of Singapore, Singapore
- Harold Soh, Prof., National Univ. of Singapore, Singapore

The author also would like to send gratitude to her spouse for the support through author's academic journey.

Contents

List of Figures

Chapter 1

Introduction

Robust tactile sensing is widely known as crucial for effective robotic manipulation. Modern robots can be equipped with soft pads that deform under contact with objects. This deformation provides vital information about interactions between the robot and its environment. This is the fundamental phenomenon powering the research in tactile sensing. By measuring and interpreting these deformations, robots can adapt to handle the objects dexterously and securely at the same time.

Accurate measurement of the contact properties with surface deformation remains a complex challenge. One powerful strategy is to replicate the human fingertip to achieve the same or larger amounts of useful data from a sensor. Since the 1970s, researchers have developed a range of artificial tactile sensors starting from piezo-resisting load cells composed into arrays [1] to more advanced optical-tactile systems that are on par and even outperform the human tactile capabilities [2].

While many existing tactile sensors primarily focus on measuring pressure, studies in continuum mechanics [3] and human tactile perception [4] underscore the importance of capturing shear strain. Shear provides valuable insights into surface-level interactions—such as slip and tangential motion—that are critical for achieving stable and adaptive grasping. However, designing tactile sensors that robustly detect shear strain across multiple loading cycles is difficult. For instance, optical sensors that rely on embedded markers often degrade over time as the protective outer layer wears down, introducing noise and reducing reliability. Such degradation leads to

frequent replacements and increased maintenance costs.

To address these limitations, NUSense was introduced - an optical tactile sensing principle based on shear strain detection. Building on previous work [5], a sensor that uses silicone rubber dyed with color inks to quantify shear deformation was presented. Spline interpolation is applied to reconstruct the surface deformation from camera images, enabling robust estimation of shear strain.

The primary contributions of this work are: 1) a tactile sensing principle based on shear strain, 2) a robust sensor design and fabrication process, and 3) a B-spline-based algorithm to extract tactile data from camera images. The remainder of this report is organized as follows: Chapter 2 provides an overview of optical tactile sensing. In Chapter 3, the NUSense sensing principle was described in detail in Section 3.1, the sensor design and fabrication process was described in Section 3.2. Section 3.3 discusses the image processing pipeline. In Chapter 4, the properties and experimental results of the sensor on force measurements and contact localization were presented. Finally, Chapter 5 concludes the thesis report with final notes and future work proposal.

Chapter 2

Related works

As robots become more integrated into human environments, it becomes increasingly important for them to safely and reliably manipulate everyday objects. Tactile sensors are considered essential for enabling dexterous object manipulation and thus, it is important to develop a general-purpose tactile sensor capable of meeting the demands of diverse manipulation tasks.

Optical or vision-based tactile sensors (VBTS), particularly those with soft pads, have emerged as promising candidates due to their versatility and effectiveness in various applications. These sensors have gained significant attention over the past decades, with researchers developing various hardware and software prototypes that enable robots to acquire direct feedback from contact. Unlike conventional piezoresistive, piezoelectric, and capacitive sensors, VBTS provide higher spatial resolution, remain unaffected by electromagnetic interference, and offer expanded capabilities beyond force perception, such as texture recognition, shape detection, 3D reconstruction, and slip detection, by integrating multiple modalities within a single sensor [6].

Leading advancements in the field include sensors such as GelSight [7], GelForce [8], TacTip [9], FingerVision [10], and Digit [11]. The fundamental components of most VBTS designs include a soft sensing skin for contact, an illumination source (typically LEDs), a camera, and a 3D-printed casing to house the system [12].

The soft skin is generally made of commercially available silicone materials, and depending on the application, it can incorporate markers, patterns, or a protective

layer. In force perception and slip detection scenarios, 2D or 3D markers are often employed, with 3D-shaped or multi-colored markers that enable the measurement of shear forces [6]. For applications like texture classification and shape reconstruction, markerless skins are preferred to avoid visual obstruction of tactile images. However, in the approach inspired by [5], a 2D biomimetic grid pattern was used that maintains the integrity of texture and shape data while simultaneously serving as the primary feature for the perception of normal, shear, and torsional forces, without compromising spatial resolution.

Although the elasticity of silicone rubber provides resilience to normal loading cycles, optical sensors with embedded markers often suffer from wear and degradation of the outer protective layer. Once damaged, these layers cause noise in the sensor's signal and reduce measurement reliability. To overcome this, replaceable elastomer layers were introduced in several designs. However, even with this solution, frequent maintenance is required.

Lighting plays a crucial role in transmitting tactile information from the deformed skin to the camera. Uniform light distribution ensures consistent performance across the sensor surface. For 3D shape reconstruction, some designs employ photometric stereo using monochromatic or colored LEDs to extract depth from shading. In other cases, light refraction inside the elastomer is used as the primary transduction mechanism, where contact is inferred from ray angle changes [13].

VBTS typically utilize compact RGB cameras to maintain a low-cost and compact form factor. Some systems have incorporated stereo or depth cameras, while others have explored neuromorphic event-based cameras for high-speed applications [14, 15, 16, 17]. Advances in computer vision and image processing have significantly improved the quality and interpretation of tactile data. Common tasks include contact segmentation, 3D surface modeling, slip detection, force estimation, and contact localization. For force estimation, marker displacement is tracked over time, and the data are processed using either mathematical models or deep learning approaches [18]. Mathematical modeling offers higher data efficiency and allows synthetic data generation in simulations, while neural networks provide more flexibility at the cost of

requiring large labeled datasets.

Despite these advances, it remains difficult to build VBTS that combine high resolution, shear sensing, robustness, and compatibility with multiple manipulation tasks in a single unit. Marker placement can reduce visibility, and damaged outer layers affect long-term performance.

To address these challenges, NUSense was introduced—a vision-based tactile sensor that directly detects shear strain using a unique biomimetic pattern and an algorithm based on B-spline surface modeling. The sensor's layered construction protects the internal structure from mechanical disturbances, enhancing its durability over extended use. It is the first VBTS to integrate a shear-based sensing principle into a compact and robust design, as illustrated in Chapter 3 Fig. 3-2.

In earlier developments within our research group, around 10,000 cycles of mechanical loading were required to train deep learning models that could reliably interpret optical tactile data [19, 5, 20]. These results emphasized the importance of sensor durability and the role of machine learning in enhancing tactile data interpretation, particularly for complex tasks like shear estimation and texture recognition.

In summary, VBTS have evolved into powerful tools for robotic manipulation. Yet, their widespread use in real-world environments still depends on solving key problems related to marker robustness, multimodal integration, and wear resistance. NUSense provides a step toward resolving these limitations through a novel sensing principle and improved structural design.

Chapter 3

NUSense

The development of the NUSense tactile sensor was driven by the need for a robust, shear-sensitive vision-based tactile system that overcomes common limitations in existing tactile sensors. As discussed in Chapter 2, many optical tactile sensors rely on embedded markers or membrane-based structures, which are prone to degradation over repeated contact cycles. Additionally, capturing shear strain—an important mechanical component of touch—remains difficult to achieve reliably across varied contact conditions.

Inspired by the layered architecture and strain sensitivity of human glabrous skin, NUSense introduces a novel biomimetic sensing principle based on surface deformation and shear estimation. Unlike previous approaches that depend heavily on pressure mapping or marker displacement, NUSense uses colored elastomeric layers and geometric pattern deformation to reconstruct contact-induced shear. This design enables high-resolution tactile imaging while improving sensor durability and simplifying fabrication.

The overall workflow of NUSense is presented in Figure 3-1. It includes three key stages: (a) deformation capture through indentation on a soft patterned surface, (b) image acquisition from a built-in camera under the elastomer, and (c) surface reconstruction using B-spline interpolation techniques to quantify shear deformation.

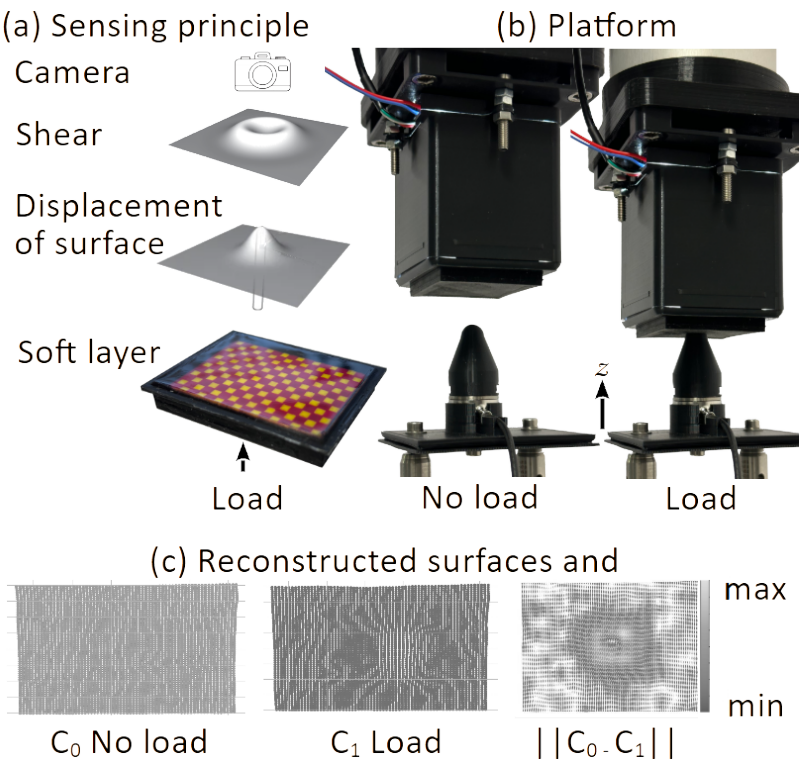

Figure 3-1: a) Sensing Mechanism: The system detects surface deformation resulting from a localized, symmetric indentation (a point load). The top layer is a silicone-based elastomer infused with colored dyes. When indented, the resulting deformation pattern is visually captured by an underlying image sensor. b) Setup: A robotic arm is equipped with the tactile sensor and a precision indenter used to apply controlled point loads. c) Surface Modeling: B-spline patches are used to reconstruct the surface geometry from captured images, both in its undeformed (resting) and deformed states. Shear deformation appears as a ring-like (annular) region. The amount of shear is quantified by measuring the displacement between the two reconstructed surfaces, using their respective B-spline control meshes, C_0 (rest) and C_1 (loaded).

3.1 Shear Strain Sensing Principle

Although vision-based tactile sensors have advanced considerably, it is essential to recognize that the sense of touch is governed by contact mechanics—an area that differs fundamentally from optical principles. As V. Hayward insightfully stated: "*Haptics and tactile sensing is thus the province of mechanics*" [21].

3.1.1 Contact mechanics of stresses and strains in human glabrous skin.

In the human somatosensory system, mechanoreceptors detect and transmit information about tissue displacement to the brain. These sensory signals are influenced by the mechanical behavior of soft tissues under external loads. While the exact relationship between these signals and skin deformation is complex and outside the scope of this work, a simplified representation of glabrous skin under normal loading is shown in Figure 3-2a. It is thought that the ridges within the epidermis contribute to sensing shear strain, which plays a key role in the perception of sharp edges [22]. These ridges form an interlocking structure between the epidermis and dermis, where vertical displacement of the skin surface causes tangential motion within the deeper layers, resulting in shear strain, γ.

When a mechanical load is applied to the skin, it causes the surface of the epidermis to deform [23]. If we model the skin as a uniform, incompressible material, a concentrated force $F \cdot \delta(x, y) \in \Re^3$ applied at the point $(0, 0)$ produces a displacement $\boldsymbol{u}(x, y, z) \in \Re^3$ at position (x, y) and depth z. The skin's response to this force, described by $g(x, y)$, can be approximated as a low-pass filter, which spreads out the effect of the force over an area. This process is similar to applying a Gaussian blur with width ε, denoted as $\phi_\varepsilon(x, y)$ (see surface deformation in Figure 3-1a). To put differently, sensing a touch on soft skin begins by smoothing or spreading the pressure across the surface.

The distribution of stress on the skin surface can be described using a convolution: $\sigma(x, y) = (f * g)(x, y)$, where $f(x, y)$ represents the applied pressure and $g(x, y)$ models how the soft tissue spreads that pressure [24]. When a small, focused force is applied, it creates a stress pattern that causes shear deformation, typically forming a ring-like (annular) area on the surface (see Figure 3-1a) [23]. This shear effect can be understood through a simplified example: when normal pressure is applied to soft silicone rubber, shear stress appears along two crossing lines, labeled AA' and BB' in Figure 3-2b. These tangential forces cause sideways (tangential) movements in the

material, known as shear strain. According to Hooke's law, the shear strain at the surface level ($z = 0$) can be approximated by:

$$\gamma(x) \simeq \frac{3}{E}\frac{d}{dx}(\sigma * \phi_\varepsilon)(x), \tag{3.1}$$

where E is the Young's modulus of the material. This equation shows that shear strain is related to the rate of change of the stress distribution, smoothed by a Gaussian filter $\phi_\varepsilon(x)$, and scaled by the stiffness of the material.

3.1.2 Implications for Soft Pad Design

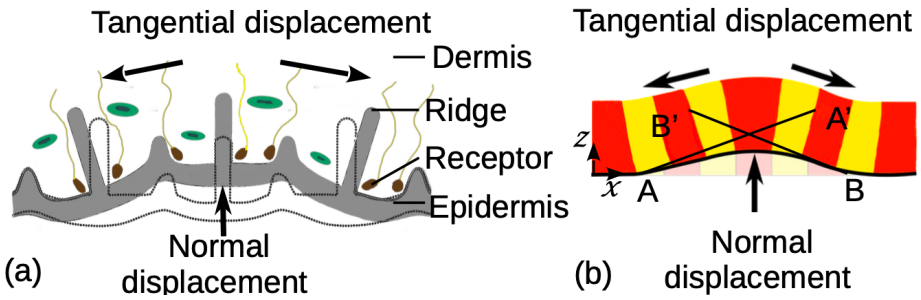

Figure 3-2: Bio-mimetic sensing principle: a) Human glabrous skin. The epidermis has ridges projecting into the dermis in the human glabrous skin. b) The structure and mechanics of the artificial sensing skin.

The skin model discussed earlier follows the principles of continuum mechanics, which apply well to materials like rubber that are nearly incompressible. The soft pad used in NUSense sensor is made of several layers of silicone rubber, each with different properties. As explained in the next section, this layered pad is mounted on top of a camera with built-in backlighting. To make the shear deformation more visible in the images, one of the silicone layers is tinted using colored inks.

As shown in Figure 3-2b, the sensing layer contains a repeating pattern of red and yellow blobs. When the soft material is pressed, the tangential movement causes these blobs to shift. The borders between adjacent blobs function like the ridges in human skin (Figure 3-2a), which also respond to shear. Around the area where contact occurs, the material stretches outward due to tensile stress, and this deformation is captured by the camera placed underneath the colored layer.

To measure this deformation, the system tracks specific geometric features within the pattern. These features are physically part of the pattern, similar to how the ridges in human skin are connected to mechanoreceptors (Figure 3-2a). By using this design, the sensor becomes more reliable across different contact scenarios. This shear-based sensing method provides improved robustness compared to our earlier approaches [5].

To accurately capture tactile information, the sensor must provide clear signals with enough spatial resolution to detect fine details of contact. This requires a camera with suitable resolution, as well as a color grid that contains distinctive visual features to identify even small deformations. According to earlier studies, the top layer of the sensor should be both durable and sensitive. If this outer layer is too thick, it may reduce sensitivity to surface deformation [24]. Therefore, careful balance between mechanical strength and sensitivity is essential in the design of the soft sensing pad.

3.2 Materials and Manufacture

3.2.1 Materials

The NUSense sensor was built using widely available, off-the-shelf components. A USB webcam (Zerodis, HBVCAM-3M2111WA V22) was used to capture images of the color pattern shifts. Illumination was provided by surface-mount white LEDs (type 3528), which were mounted on a printed circuit board and powered at 100 mA each. Light from these LEDs was diffused and directed through four edges of a 3 mm-thick Plexiglass panel, ensuring even illumination across the sensing area. The soft silicone pad was firmly attached to this transparent glass base to hold the color pattern in place.

The sensor's outer casing—including the camera mount, base, and cover—was 3D printed using Polylactic Acid (PLA) filament. The topmost layer of the pad was molded from clear silicone rubber (Smooth-On, Sorta-Clear 18). Below this, the sensing layer containing the colored pattern was carefully cast. A soft, transparent

gel (Techsil, RTV27905) was added as the middle layer, and a thin coat of PDMS (Polydimethylsiloxane) was applied on top to secure the soft structure to the glass plate.

Figure 3-3a shows an exploded view of the sensor's internal components. The soft elastomer pad is clamped between the upper lid and the base. The camera, LED board, and light-guiding glass panels are mounted to a shared support. To prevent movement that could cause incorrect readings, the base was rigidly fixed to the camera housing. At the same time, the design allows easy disassembly, using screws and bolts, for maintenance or modification.

The full sensing area measures 55×43 mm, with an effective contact region of 50×38 mm. The camera lens is positioned at a focal distance of 55 mm from the elastomer surface. The 3D-printed base is 1.5 mm thick to block external light and ensure stable internal illumination (Figure 3-3b).

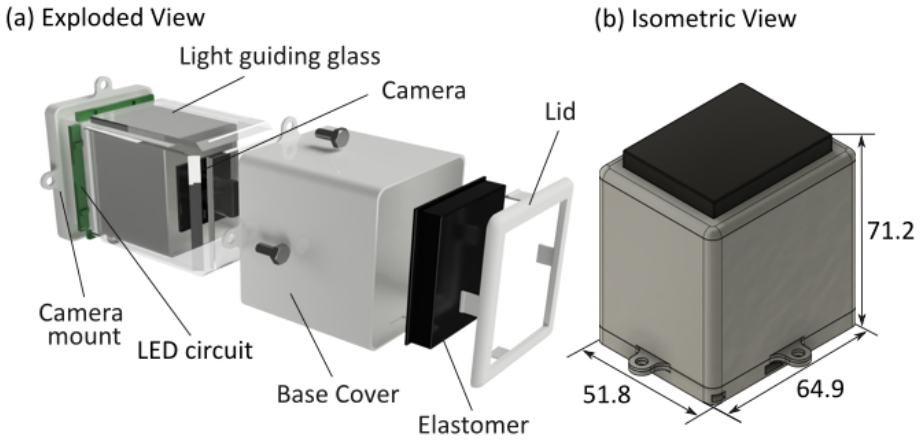

Figure 3-3: Assembly of NUSense tactile sensor with a camera and elastomer. (a) Exploded view and (b) isometric view of the NUSense. All measurements are in millimeters.

3.2.2 Manufacturing Process

The soft pad of the NUSense sensor is built step-by-step, with each silicone layer added one at a time. The full process is illustrated in Figure 3-4a. For every layer, the two components of the selected silicone rubber (parts A and B) are mixed with

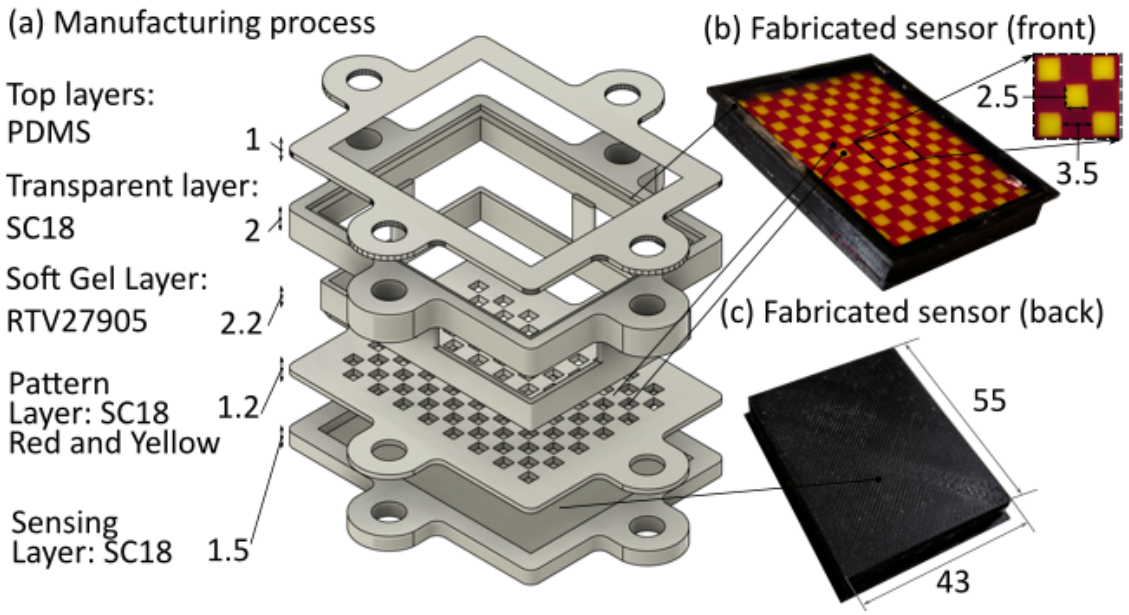

Figure 3-4: The silicone molding-based fabrication of NUSense. (a) Manufacturing process with all molding layers, (b) front and (c) back of the fabricated elastomer. All measurements are in millimeters. SC18 is Sorta-Clear 18.

the appropriate colored ink before casting.

The first step is to create the base sensing layer using black silicone rubber. After that, the patterned color layer is made in two stages: (1) yellow-colored silicone is placed into a patterned mold, and (2) once the mold is removed, red-colored silicone is poured over the remaining space to complete the pattern. When the colored layer is finished, a soft transparent gel (Soft Clear Gel) is poured to a height of 2.2 mm.

Next, a clear top layer is cast directly on top of the gel to seal it in place. Then, a black-dyed outer layer is added around the edges of the sensor to protect it from dust and surface wear. Finally, a thin PDMS layer is applied on top of the transparent surface to secure the entire elastomer structure to the glass base.

The black edge layer includes slightly raised sections (approximately 1.5 mm high) that allow the pad to be held in place mechanically. The front and back views of the finished elastomer are shown in Figures 3-4b and 3-4c.

3.3 Methodology

In this section, the shear deformation of the artificial tactile surface in the NUSense sensor, as introduced in Section 3.1, is quantitatively estimated. First, the background of B-spline surface modeling—used to represent the deformation—is explained. Then, the complete image processing pipeline is presented, including tactile image acquisition, control point extraction, and computation of the final deformation metric.

3.3.1 B-Spline Surface

The deformation of the soft sensing surface, illustrated in Figure 3-1a, is modeled using a B-spline surface representation. This surface is mathematically defined as:

$$\mathbf{S}(u,v) = \sum_{i=0}^{n} \sum_{j=0}^{m} N_{i,p}(u) M_{j,q}(v) \mathbf{P}_{i,j} \tag{3.2}$$

In this expression, $\mathbf{S}(u,v)$ denotes the resulting surface, and $\mathbf{P}i,j$ are the control points, which are organized in a grid. The terms $Ni,p(u)$ and $M_{j,q}(v)$ refer to the B-spline basis functions of degrees p and q, respectively, applied over the normalized parameters $u, v \in [0,1]$. The number of control points in the u and v directions is indicated by n and m. Additional background on the theory behind B-spline surfaces can be found in [25].

To create a smooth surface, a fine grid over the u and v domain is sampled. The control points needed for this construction are obtained from the tactile images, as described in the following subsection.

3.3.2 NUSense Data Processing

Preprocessing

The raw image obtained from the sensor covers a wide field of view, as captured by a fisheye lens (Figure 3-5a). To correct the distortion introduced by the lens, a camera matrix is applied. This matrix is calculated based on intrinsic camera parameters

and distortion coefficients. As a result, a corrected or undistorted image, denoted $\mathbf{I}$, is produced. This image is later used for extracting control points (see Figure 3-5b).

Algorithms for Control Point Extraction

The extraction process begins by selecting a region of interest from the undistorted image $\mathbf{I}$, using specified coordinates and dimensions (x, y, width, height). This cropped region is then converted into a grayscale image. The algorithm for control point extraction is outlined in Algorithm 1.

To enhance relevant features while reducing noise, a bilateral filter is applied. Edge information is then detected using the Sobel operator. The resulting image is thresholded to form a binary mask. This binary image undergoes morphological processing—specifically dilation followed by erosion—to close small gaps and eliminate unwanted noise. These steps ensure well-defined regions suitable for contour detection.

Contours are detected, and polygons representing quadrilateral shapes are extracted, as shown in Figure 3-5c. Then, the corners of adjacent quadrilaterals are located, and the midpoints between them are calculated. These midpoints, represented as $\mathbf{P}$ in Figure 3-5d, are used to form the grid of control points needed for constructing the B-spline surface as defined in equation (3.2).

Sampling from the B-Spline Surface

Once the control points $\mathbf{P}$ are identified, they are fitted to the B-spline surface described in subsection 3.3.1 to construct the surface function $S(u, v)$. From this surface, a set of evaluation points is sampled: $\mathbf{s} \sim S(u, v)$, where $\mathbf{s} \in \mathbb{R}^{3\times K}$ represents a vector containing K sampled points in 3D space.

Metrics

To evaluate the contact interaction on the tactile sensor, a metric based on shear deformation is defined. This is derived from the shear strain concept described in equation (3.1), using the B-spline surface control points introduced in equation (3.2).

Definition 1 (Shear Strain) *Let* $\mathbf{s}^{(ref)}$ *and* $\mathbf{s}$ *be the sampled surface points from the reference* S^{ref} *and target* S *B-Spline surfaces, respectively. Then the* shear strain γ_{ss} *of the touch is defined as a scaled L2-norm:*

$$\gamma_{ss} = \alpha \sum_{i=1}^{K} ||s_i - s_i^{ref}||_2 \tag{3.3}$$

where α *is a constant scaling parameter.*

In the implementation, both u and v directions are set to linear B-spline degree ($p = q = 1$), and the scaling factor is defined as $\alpha = 18000^{-1}$. The B-spline surface is assumed to lie on a 2D projection plane. The total number of control points is determined by the number of quadrilaterals visible in the tactile image, set as $m = n = 164$.

Examples of the reconstructed surfaces corresponding to $\mathbf{s}$ and $\mathbf{s}^{(\text{ref})}$ are presented in Figure 3-5e and 3-5f, respectively. A visual explanation of the shear strain metric, as described in equation (3.3), can also be seen in Figure 3-1c. All control point extraction and surface computations were implemented using Python and the OpenCV library.

Algorithm 1 Control Point Extraction

Require: Undistorted image $\mathbf{I}$, width w, height h, top-left corner x, y for RoI, and checkerboard threshold c_{th}

0: /* *Extract Region of Interest* */
0: $\mathbf{I}_{\text{crop}} \leftarrow \text{CROP}(\mathbf{I}, x, y, w, h)$
0: $\hat{\mathbf{I}}_{\text{grey}} \leftarrow \text{img2grey}(\mathbf{I}_{\text{crop}})$
0: /* *Filter by enhancing and morphology* */
0: $\mathbf{I}_{\text{grey}} \leftarrow \text{CLAHE}(\hat{\mathbf{I}}_{\text{grey}})$
0: $\mathbf{I}_{\text{filter}} \leftarrow \text{BilateralFilter}(\mathbf{I}_{\text{grey}})$
0: $\mathbf{I}_{\text{sobel}} \leftarrow \text{SOBEL}(\mathbf{I}_{\text{filter}})$
0: $\mathbf{I}_{\text{dilation}} \leftarrow \text{DILATION}(\mathbf{I}_{\text{sobel}})$
0: $\mathbf{I}_{\text{erosion}} \leftarrow \text{EROSION}(\mathbf{I}_{\text{dilation}})$
0: /* *Extract Control Points* */
0: $\mathbf{C} \leftarrow \text{FindContour}(\mathbf{I}_{\text{erosion}})$
0: $\mathbf{P} \leftarrow \{\}$
0: **for all** $c_i \in \mathbf{C}$ **do**
0: **for all** $c_j \in \mathbf{C}$ **do**
0: **if** $\text{dist}(c_i, c_j) \leq c_{\text{th}}$ **then**
0: $\hat{\mathbf{P}} \leftarrow \text{CollectClosestMidpoints}(c_i, c_j)$
0: **for all** $\hat{p} \in \hat{\mathbf{P}}$ **do**
0: $\mathbf{P} \leftarrow \mathbf{P} \cup \{\hat{p}\}$
0: **end for**
0: **end if**
0: **end for**
0: **end for**
0: **return** $\mathbf{P}$ {Control Points} =0

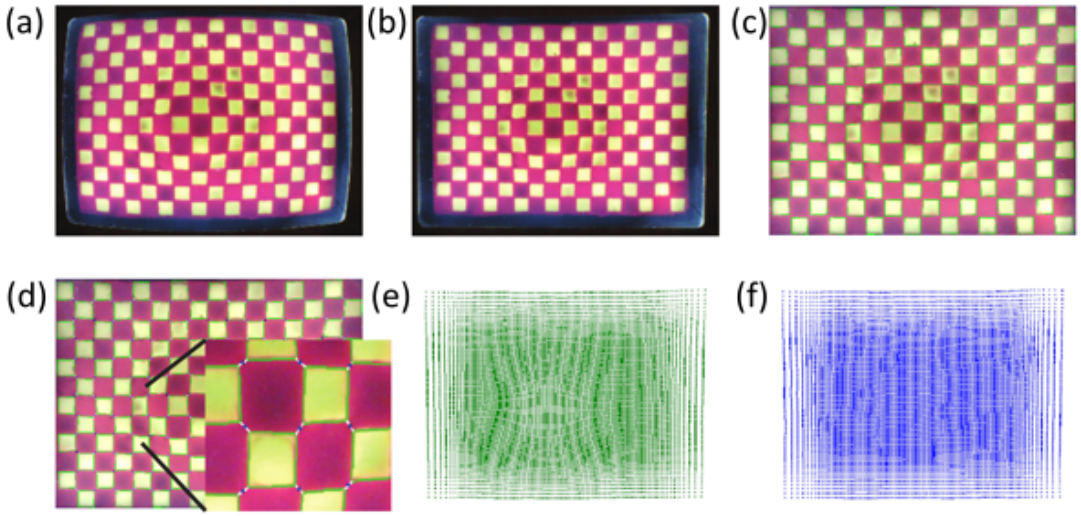

Figure 3-5: Tactile image processing workflow: (a) Raw tactile image captured using a fisheye lens camera, (b) Corrected image after lens distortion removal, (c) Detected quadrilateral polygons surrounding yellow pattern markers, (d) Midpoints between adjacent polygons extracted as B-spline control points (magnified view shown), (e) Sampled points from the deformed (target) B-spline surface, (f) Sampled points from the reference (resting) B-spline surface.

Chapter 4

Experiments

4.1 Robotic Setup

We attached our NUSense tactile sensor onto a robot arm (Universal Robots; repeatability ±0.1 mm). Edge- and point-protruding indenters were secured on top of an optical breadbaord with mounting plate (Thorlabs). An industrial force/torque sensor (hex21, Wittenstein) was fixed between the plate and the indenters to calibrate the sensor output to SI units (Figure 4-1). The robot arm was controlled using the position servoing mode at 125 Hz. The 6 axis force/torque sensor was sampled at the same rate to obtain ground truth force measurements. The communication interface with the workstation (Intel Xeon E5620 2.40 Ghz, 4 GB DDR3 memory, Ubuntu Linux) was implemented using Robot Operating System 1 (ROS). Camera images were sampled at 12 Hz.

Each indenter was positioned to protrude the NUSense sensor at desired locations, which were manually set at the geometric center. The maximum depth of protrusion corresponded to a force of 8 N.

4.2 Normal Force Estimation

To evaluate the ability of NUSense to estimate normal force, indentation experiments were conducted using two tools: a flat-tip indenter (Figure 4-1b) and a round-tip

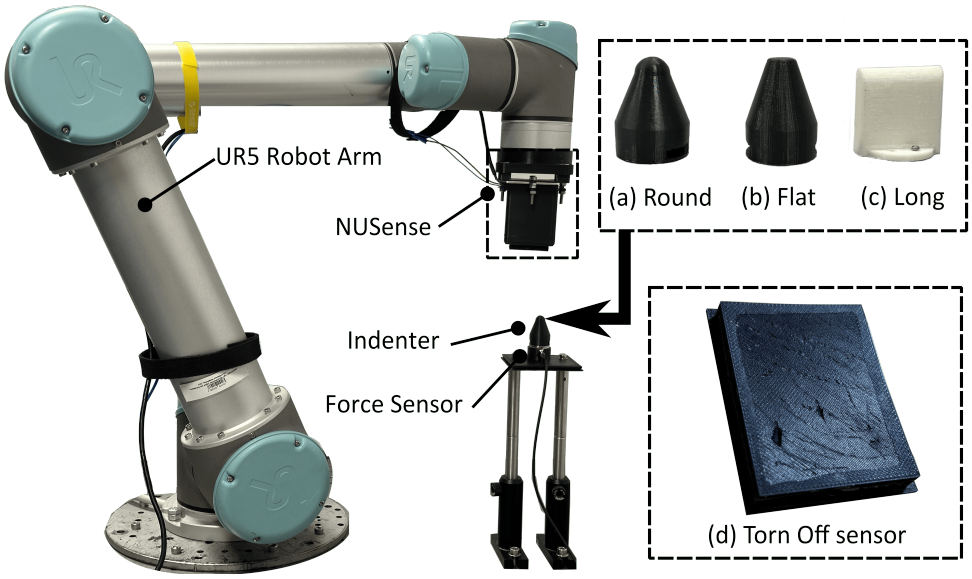

Figure 4-1: Experimental Setup. Indenters with three different areas of contact. Normal force response in the ranges 1 N to 3 N and 3 N to 8 N was obtained by (a) round and (b) flat tips, respectively. (c) Long tip was used for edge detection. (d) Torn off elastomer sensor.

indenter (Figure 4-1a), both having a tip radius of 5 mm. The flat indenter applied force up to 3 N, while the round indenter reached up to 8 N. The corresponding shear strain values, calculated using equation (3.3), were recorded and plotted in Figure 4-2g. A linear relationship between force and shear strain was observed in the range of 1 N to 8 N, with the fitted line expressed as $F = 3.09\gamma_{ss} - 1.14$. Forces below 1 N did not result in significant deformation, and forces above 8 N were avoided to prevent potential damage to the sensor.

4.3 Single Contact Localization

The shear strain pattern for both indenters formed an annular shape centered at the point of contact. To assess contact localization accuracy, a 6 N force was applied at 24 discrete positions across the sensor surface, spaced 6.4 mm apart in the x-direction and 7 mm in the y-direction. Figure 4-2e displays the estimated contact points across three trials. The sensor demonstrated reliable localization, with a slight shift observed along the vertical axis. The root mean square (RMS) localization error was measured

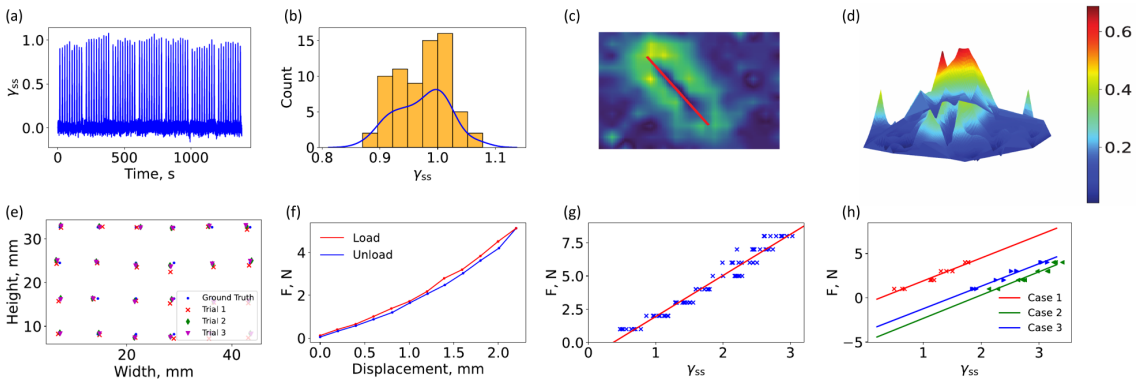

Figure 4-2: Experimental Results: (a) Shear strain versus time (b) Histogram of the maximum deformations for each touch in the robustness experiment (c) Shear strain projection on 2D (d) Corresponding 3D visualization (e) Single indent touch localization (f) Hysteresis (g) Force calibration (h) Three cases for *tore-off* sensor configuration.

at 0.50 ± 0.09 mm.

4.4 Hysteresis

Due to the viscoelastic nature of the silicone rubber, a hysteresis effect was observed between the loading and unloading phases. This effect is shown in Figure 4-2f, where the round-tip indenter was pressed at a constant speed of $0.5, \text{mm/s}$. As expected, the degree of non-linearity increased with softer materials. Therefore, a trade-off must be considered between sensitivity and bandwidth, which is essential for real-time force control.

4.5 Robustness

The consistency of sensor output under repeated mechanical loading was tested by programming the robot arm to apply 70 cycles of pressure. The resulting maximum shear strain for each touch is presented in Figure 4-2a, and the variance is shown in Figure 4-2b. Low variability across cycles confirmed the robustness and repeatability of the sensor's response.

4.6 Edge Detection

The ability of the sensor to recognize edge contacts was also investigated. A long edge-shaped indenter applied an 8 N force at various orientations relative to the x-axis. The resulting shear strain pattern (Figure 4-2c) was analyzed using Principal Component Analysis (PCA) on the most deformed points. The principal direction (red line) corresponded to the orientation of the edge and aligned approximately 60° clockwise. A 3D visualization of the shear region is presented in Figure 4-2d, where it can be seen that the center contact area remains undeformed, while the surrounding region clearly shows shear displacement.

4.7 Force Estimation Under Sensor Damage

Since the outermost layer of the soft pad may degrade when interacting with sharp objects, the sensor's performance under damage was tested. The soft layer was intentionally cut, as shown in Figure 4-1d. To assess whether sensor functionality could be preserved, three different cases were examined: two with undamaged but separately fabricated pads (Cases 1 and 2), and one with a torn outer layer (Case 3).

Force estimates for applied pressures of 1, 2, 3, and 4 N are shown in Figure 4-2h. In all cases, a linear trend was maintained, similar to the calibration test. Minor variations in bias between trials were attributed to fabrication inconsistencies in Cases 1 and 2 and the mechanical damage in Case 3. Nonetheless, the sensor maintained its ability to detect force, even with a damaged surface.

Chapter 5

Conclusion and Future Work

In this study, the NUSense optical tactile sensor was introduced, utilizing shear strain detection for implicit estimation of applied force. Unlike conventional methods, the proposed approach relied on the observation of shear deformation through a vision-based system to infer contact forces. The sensing principle was validated through a series of experiments, in which the sensor demonstrated reliable performance in estimating normal force, localizing contact points, and detecting edge directions, all with high repeatability and robustness.

Certain limitations were acknowledged in this work. The soft pad was modeled as an isotropic material composed of silicone rubber, and it was assumed that the material remained within its elastic range without sustaining puncture damage. Future efforts will be directed toward overcoming these limitations by refining the material composition and enhancing the algorithms used for deformation analysis.

Bibliography

[1] Z. Stojiljkovic and J. Clot, "Integrated behavior of artificial skin," *IEEE Trans. on Biom. Eng.*, vol. 24, no. 4, pp. 396–399, 1977.

[2] J. Lloyd and N. F. Lepora, "Pose-and-shear-based tactile servoing," *IJRR*, vol. 43, no. 7, pp. 1024–1055, 2024.

[3] S. Ricker and R. Ellis, "2-d finite-element models of tactile sensors," in *IEEE ICRA*, 1993, pp. 941–947.

[4] R. Kikuuwe, A. Sano, H. Mochiyama, N. Takesue, and H. Fujimoto, "Enhancing haptic detection of surface undulation," *ACM Trans. Appl. Percept.*, vol. 2, no. 1, p. 46–67, jan 2005.

[5] D. Baimukashev, Z. Kappassov, and H. A. Varol, "Shear, torsion and pressure tactile sensor via plastic optofiber guided imaging," *IEEE RA-L*, vol. 5, no. 2, pp. 2618–2625, 2020.

[6] K. Shimonomura, "Tactile image sensors employing camera: A review," *Sensors*, vol. 19, no. 18, p. 3933, 2019.

[7] W. Yuan, S. Dong, and E. H. Adelson, "Gelsight: High-resolution robot tactile sensors for estimating geometry and force," *Sensors*, vol. 17, no. 12, p. 2762, 2017.

[8] K. Sato, K. Kamiyama, N. Kawakami, and S. Tachi, "Finger-shaped gelforce: sensor for measuring surface traction fields for robotic hand," *IEEE Transactions on Haptics*, vol. 3, no. 1, pp. 37–47, 2009.

[9] B. Ward-Cherrier, N. Pestell, L. Cramphorn, B. Winstone, M. E. Giannaccini, J. Rossiter, and N. F. Lepora, "The tactip family: Soft optical tactile sensors with 3d-printed biomimetic morphologies," *Soft robotics*, vol. 5, no. 2, pp. 216–227, 2018.

[10] Y. Zhang, Z. Kan, Y. A. Tse, Y. Yang, and M. Y. Wang, "Fingervision tactile sensor design and slip detection using convolutional lstm network," *arXiv preprint arXiv:1810.02653*, 2018.

[11] M. Lambeta, P.-W. Chou, S. Tian, B. Yang, B. Maloon, V. R. Most, D. Stroud, R. Santos, A. Byagowi, G. Kammerer *et al.*, "Digit: A novel design for a low-cost compact high-resolution tactile sensor with application to in-hand manipulation," *IEEE RA-L*, vol. 5, no. 3, pp. 3838–3845, 2020.

[12] S. Zhang, Z. Chen, Y. Gao, W. Wan, J. Shan, H. Xue, F. Sun, Y. Yang, and B. Fang, "Hardware technology of vision-based tactile sensor: A review," *IEEE Sensors*, vol. 22, no. 22, pp. 21 410–21 427, 2022.

[13] K. Shimonomura, "Tactile image sensors employing camera: A review," *Sensors*, vol. 19, no. 18, 2019.

[14] K. Kumagai and K. Shimonomura, "Event-based tactile image sensor for detecting spatio-temporal fast phenomena in contacts," in *IEEE WHC*, 2019, pp. 343–348.

[15] R. Muthusamy, X. Huang, Y. Zweiri, L. Seneviratne, and D. Gan, "Neuromorphic event-based slip detection and suppression in robotic grasping and manipulation," *IEEE Access*, vol. 8, 2020.

[16] A. Rigi, F. Baghaei Naeini, D. Makris, and Y. Zweiri, "A novel event-based incipient slip detection using dynamic active-pixel vision sensor (davis)," *Sensors*, vol. 18, no. 2, p. 333, 2018.

[17] B. Ward-Cherrier, N. Pestell, and N. F. Lepora, "Neurotac: A neuromorphic optical tactile sensor applied to texture recognition," in *IEEE ICRA*, 2020, pp. 2654–2660.

[18] S. Li, Z. Wang, C. Wu, X. Li, S. Luo, B. Fang, F. Sun, X.-P. Zhang, and W. Ding, "When vision meets touch: A contemporary review for visuotactile sensors from the signal processing perspective," *arXiv preprint arXiv:2406.12226*, 2024.

[19] Z. Kappassov, D. Baimukashev, Z. Kuanyshuly, Y. Massalin, A. Urazbayev, and H. A. Varol, "Color-coded fiber-optic tactile sensor for an elastomeric robot skin," in *2019 International Conference on Robotics and Automation (ICRA)*, 2019, pp. 2146–2152.

[20] D. Mukashev, N. Zhuzbay, A. Koshkinbayeva, B. Orazbayev, and Z. Kappassov, "Photoelasticfinger: Robot tactile fingertip based on photoelastic effect," *Sensors*, vol. 22, no. 18, 2022.

[21] V. Hayward, "Tactile illusions," *Scholarpedia*, vol. 10, p. 8245, 2015.

[22] Q. Wu and J. Li, "Distribution characteristics and correlation of edge sharpness threshold and contact area," *IEEE Transactions on Haptics*, pp. 1–11, 2024.

[23] J. Platkiewicz, H. Lipson, and V. Hayward, "Haptic edge detection through shear," *Scientific reports*, vol. 6, no. 1, p. 23551, 2016.

[24] M. Shimojo, "Mechanical filtering effect of elastic cover for tactile sensor," *IEEE Trans. on Rob. and Autom.*, vol. 13, pp. 128–132, 1997.

[25] W. J. Gordon and R. F. Riesenfeld, "B-spline curves and surfaces," in *Computer aided geometric design.* Elsevier, 1974, pp. 95–126.